

## **UNIT 11.10 X-ray Microprobe for Fluorescence and Diffraction Analysis**

**Gene E. Ice**  
**Metals and Ceramics Division**  
**Oak Ridge National Laboratory**  
**Oak Ridge Tennessee 37831-6118**

**Phone 423-482-6535**  
**Fax 423-574-2744**

**Email [gei@ornl.gov](mailto:gei@ornl.gov)**

**Key Terms: Nondestructive analysis; minimum detectable limit; trace  
element; strain/stress; texture; x-ray microbeam**

**Floppy disks include versions of the tutorial with and without  
imbedded figures. Most of the files are in Microsoft word 6.0 but some  
are in Powerpoint. The files were created on a PowerMac. The files for  
the figures are labeled according to their figure number.**

# UNIT 11.10 X-ray Microprobe for Fluorescence and Diffraction Analysis

## INTRODUCTION

X-ray diffraction (see unit 1.1) and x-ray excited fluorescence analysis are powerful techniques for the nondestructive measurement of crystal structure and chemical composition. X-ray fluorescence analysis is inherently nondestructive with orders of magnitude lower power deposited for the same detectable limit as with fluorescence excited by charged particle probes (Sparks, 1980). X-ray diffraction analysis is sensitive to crystal structure with orders-of-magnitude greater sensitivity to crystallographic strain than electron probes (Rebonato, et al. 1989). When a small-area x-ray microbeam is used as the probe, chemical composition ( $Z > 14$ ), crystal structure, crystalline texture, and crystalline strain *distributions* can be determined. These distributions can be studied both at the surface of the sample and deep within the sample (Fig. 1). Current state-of-the-art can achieve an  $\sim 1 \mu\text{m-D}$  x-ray microprobe and an  $\sim 0.1 \mu\text{m-D}$  x-ray microprobe has been demonstrated (Bilderback, et al., 1994).

Despite their great chemical and crystallographic sensitivities, x-ray microprobe techniques have until recently been restricted by inefficient x-ray focusing optics and weak x-ray sources; x-ray microbeam analysis was largely superseded by electron techniques in the 50's. However, interest in x-ray microprobe techniques has now been revived (Howells, et al., 1983; Ice & Sparks, 1984; Chevallier, et al., 1997; Riekel 1992; Thompson, et al., 1992; and Making and Using... 1997) by the development of efficient x-ray focusing optics and ultra-high intensity synchrotron x-ray sources (Buras & Tazzari, 1984; Shenoy, et al., 1988). These advances have increased the achievable microbeam flux by more than 11 orders of magnitude (Fig. 2) (Ice, 1997); the flux in a tunable  $1 \mu\text{m-D}$  beam on a "so called" 3rd-generation synchrotron source such as the APS can exceed the flux in a fixed-energy  $\text{mm}^2$  beam on a conventional source. These advances make x-ray microfluorescence and x-ray microdiffraction analysis techniques some of the most powerful techniques available for the

nondestructive measurement of chemical and crystallographic distributions in materials.

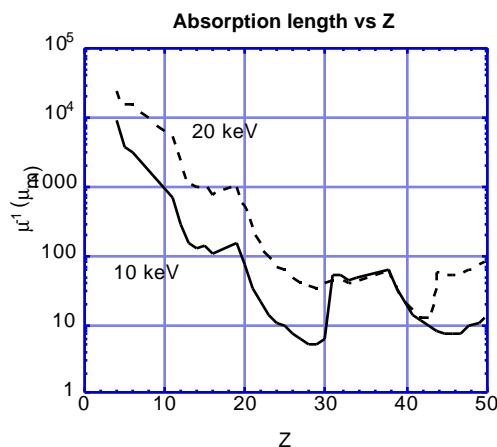


Fig. 1 Absorption depth for 10 and 20 keV x-rays as a function of elemental composition  $Z$ .

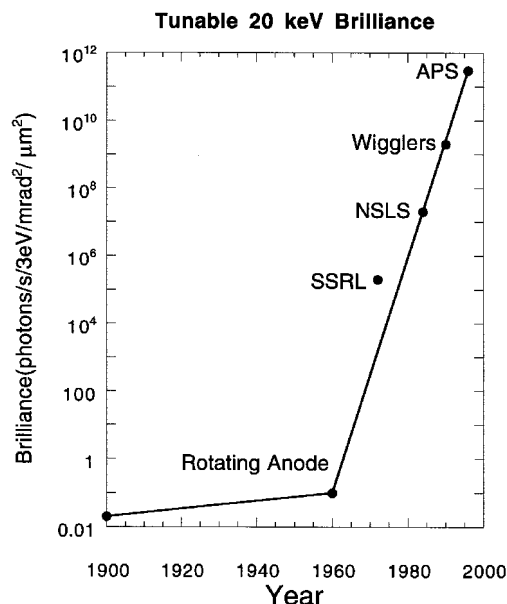


Fig. 2 X-ray brilliance over the last 100 years shows a more than 11 orders of magnitude increase since the use of hard x-ray synchrotron radiation sources began in the late 60's. Both x-ray microdiffraction and x-ray microfluorescence have brilliance ( $\text{photons/s/ev/mm}^2/\text{mrad}^2$ ) as the

figure of merit (Ice, 1997).

This unit reviews the physics, advantages, and scientific applications of hard x-ray ( $E > 3$  keV) microfluorescence and x-ray microdiffraction analysis. Because practical x-ray microbeam instruments are extremely rare, a special emphasis will be placed on instrumentation, accessibility, and experimental needs which justify the use of x-ray microbeam analysis.

### Competitive and related techniques

Despite their unique properties, x-ray microprobes are rare and the process of gaining access to an x-ray microprobe can be difficult. For many samples, alternative techniques exist with far greater availability. Destructive methods such as laser ionization with mass spectrometry (Stwalley, 1998), and atom probe (Miller, et al., 1996) methods can yield information on composition distributions. Atom probe measurements in particular can measure the atom-by-atom distribution in a small volume but require extensive sample preparation.

Auger spectroscopy (Joshi, 1998) and Rutherford backscattering (Banks, et al., 1998) techniques are other possible methods for determining elemental distributions. Auger analysis is inherently surface sensitive; whereas, Rutherford backscattering measurements can probe below the sample surface. Although these techniques are generally considered very sensitive, x-ray analysis can be even more sensitive.

The most directly comparable analysis techniques are charged particle microprobes such as electron or proton microprobes (Sparks, 1980; Anderson & Marienko, 1998; Samorjai, 1998); Cowley & Marks, 1998; Eades, 1998; and Campbell & Guelph, 1998). Whereas proton microprobes are almost as rare as x-ray microprobes, electron microprobes are widely used to excite fluorescence for chemical analysis. Electron microbeams are also used to measure crystallographic phase and texture, and strain resolution to  $2 \times 10^{-4}$  has been demonstrated (Michael & Goehner, 1993). Advanced electron microbeams can deliver  $10^{12}$ - $10^{15}$  electrons/ $\mu\text{m}^2$  and can be focused to nm-D dimensions. Electron microbeams are available at many sites within the U.S. and around the world.

Sparks (1980) has compared the relative performance of x-ray, proton and electron microprobes for chemical analysis. He specifically compared the intrinsic ability of x-ray and charged particle microprobes to detect trace elements in a matrix of other elements. He also compared their relative abilities to resolve small dimensioned features. In summary he finds that x-rays have major advantages: (1) x-rays are very efficient at creating inner shell holes; (2) x-ray excitation produces very low backgrounds; (3) beam spreading with x-rays is low; and (4) x-ray microprobe analysis requires minimum sample preparation.

A comparison of the signal-to-background for various probes is shown in Fig. 3. Monochromatic x-ray excitation produces the best fluorescence signal-to-background. Proton excitation produces signal-to-background between x-ray and electron induced fluorescence. For low Z elements proton microbeams can sometimes approach the signal-to-background of x-ray microbeams.

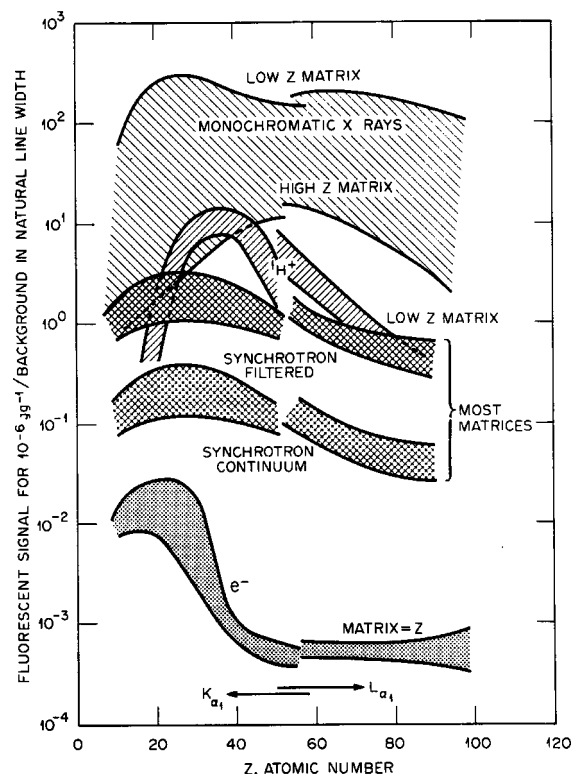


Fig. 3 Comparison of the fluorescence signal-to-background ratio for various excitation probes at a concentration of  $10^{-6} \text{ gg}^{-1}$  for an x-ray detection

system with an energy resolution of the natural linewidth (after reference 1).

A rather direct comparison of the elemental sensitivity of various microbeam probes can be made by comparing their minimum-detectable limits (MDL). We adopt the MDL definition of Sparks (1980) for fluorescence analysis,

$$C_{MDL} = 3.29C_Z \frac{\sqrt{N_b}}{N_s} . \quad (1)$$

Here  $C_{MDL}$  is the minimum detectable limit,  $C_Z$  is the mass fraction in a calibrated standard,  $N_b$  is the background counts beneath the fluorescence signal, and  $N_s$  is the net counts at the fluorescence energy. Lowest MDL results when the ratio  $\frac{N_s}{\sqrt{N_b}}$  is large (good signal-to-background and high flux), and when  $\frac{N_s}{C_Z}$  is large (efficient inner-shell hole production and high flux).

Table 1. Estimated MDL/s from reference 1 scaled to  $10^{12}$  monochromatic photons/s/ $\mu\text{m}^2$ . This comparison assumes that the matrix and trace element have similar Z and that an advanced multi-element solid-state detector is used where deadtime does not limit performance. With a low Z matrix or with an advanced crystal spectrometer the MDL can be lower.

Probe	MDL(ppm/s)
Proton	~10-100
electron	~ 5-30
filtered x-ray	~ 1- 8
monochromatic x-ray	~ 0.005-0.08

Electron and proton microprobes cannot match the achievable MDL of an advanced x-ray microprobe; compared to x rays, the inner shell hole production cross section and signal-to-background of an electron probe are too low and the proton probe flux density on the sample are too low. An advanced x-ray microprobe with  $10^{12}$  photons/s/ $\mu\text{m}^2$  has about a  $10^3$  lower MDL for most elements than a charged particle probe and can achieve the same MDL as electron probes

with  $10^4$  less energy deposited in the sample (Table 1).

For thin samples the spatial resolution of electron probes is far better than either x-ray or proton microprobes. In terms of their practical spatial resolution for thick samples; however, x-ray microprobes are competitive or superior to charged particle probes. Although electron probes can be focused to nm dimensions, beam spreading in thick samples degrades their effective resolution. For example, in a thick Al sample a nm electron probe spreads to an effective size of  $\sim 2 \mu\text{m-D}$ . In Cu and Au samples the same beam spreads to 1 and  $0.4 \mu\text{m-D}$  respectively (Ren, et al., 1997; Goldstein, 1979). Proton microprobes can be made very small, but the fluxes are so low that few instruments exist with probe dimensions approaching  $1 \mu\text{m-D}$  (Lindh, 1990; Doyle, et al., 1991).

X-ray beams are now so intense, that their flux density is approaching the maximum which can be usefully applied to most samples. For example, the estimated thermal rise of a thin target under an advanced x-ray microbeam is shown in Fig. 4. Existing x-ray microbeams have highly monochromatic flux densities approaching  $10^{12}$  photons/sec/ $\mu\text{m}^2$  and can go to  $10^{13}$ - $10^{14}$  photons/sec/ $\mu\text{m}^2$  with larger bandpass optics. With  $10^{14}$  photons/s/ $\mu\text{m}^2$ , the flux must be attenuated for most samples. Alternatively the probe area can be decreased or the dwell time on the sample can be reduced to prevent sample melting.

Despite its many advantages, however, x-ray microbeam analysis remains an emerging field with very little available instrumentation. The effort required to gain access to x-ray microbeam facilities must therefore be weighed against the benefits. X-ray microfluorescence analysis becomes justified when the MDL from other techniques is inadequate. It may also be justified when the probe must penetrate the sample surface; when the analysis must be highly non-destructive; when the analysis must be quantitative; or when the measurement must be done in the presence of air, water, or other low Z overlayer.

Microdiffraction analysis becomes justified when the strain resolution  $\Delta d/d$  must be better than  $\sim 2 \times 10^{-4}$ . Microdiffraction analysis is also justified for the study of crystallographic

properties beneath the surface of a sample for the measurement of texture in three dimensions or for non-destructive analysis of insulating samples where charge buildup can occur.

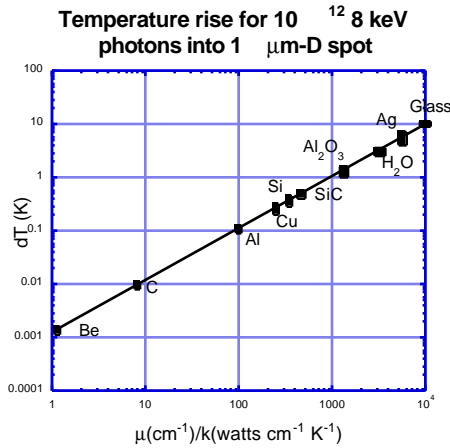


Fig. 4 Thermal rise as a function of thermal conductivity  $K$  and absorption coefficient  $\mu$  (Ice & Sparks, 1991). Note that existing x-ray microbeams have achieved  $10^{12}$  photons/sec/ $\mu\text{m}^2$  and are anticipated to reach  $10^{13}$ - $10^{14}$  photons/sec/ $\mu\text{m}^2$  for some applications.

## PRINCIPLES OF THE METHOD

A typical x-ray microbeam experiment involves three critical elements: (1) x-ray condensing or aperturing optics on a high-brilliance x-ray source, (2) a high-resolution sample stage for positioning the sample, and (3) a detector system with one or more detectors (Fig. 5). The x-ray beam axis and focal position is determined by the optics of the particular arrangement. Different locations on the specimen are characterized by moving the specimen under the fixed x-ray microprobe beam. Details of the detector arrangement and the principles involved depend strongly on the particular x-ray microprobe and on whether elemental distributions or crystallographic information is to be collected.

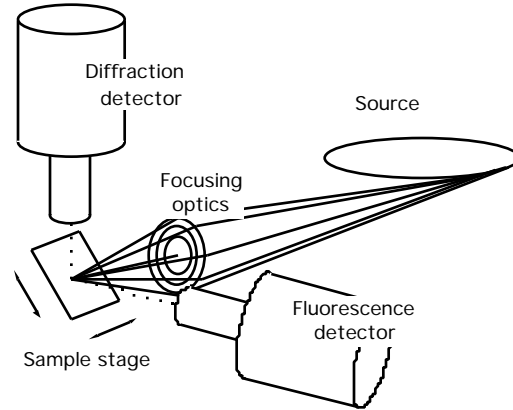


Fig. 5 Key elements of an x-ray microbeam experiment.

Both x-ray microdiffraction and x-ray microfluorescence are brilliance (photons/s/ev/ $\text{mm}^2/\text{mrad}^2$ ) limited (Ice, 1997). For x-ray microdiffraction, momentum transfer resolution is limited by spread in wavelength and angular divergence on the sample. Count-rate is limited by flux-per-unit-area. For x-ray microfluorescence, best signal-to-background occurs when the x-ray bandwidth  $\Delta E/E$  is  $\leq 3\%$  (Sparks, 1980). Spatial resolution for thick samples degrades when the divergence of the beam exceeds  $\sim 10$  mrad. The principles of x-ray microfluorescence and x-ray microdiffraction analysis are briefly outlined below.

## X-ray microfluorescence analysis

The unique advantages of x-ray probes arise from the fundamental interaction of x-rays with matter. Below the pair production threshold, the interaction of x-rays with matter is dominated by three processes: photoabsorption (photoelectric effect), elastic scattering, and inelastic (Compton) scattering (Veigele, et al., 1969). Of these three processes, photoabsorption has by far the largest cross section in the 3-100 keV range.

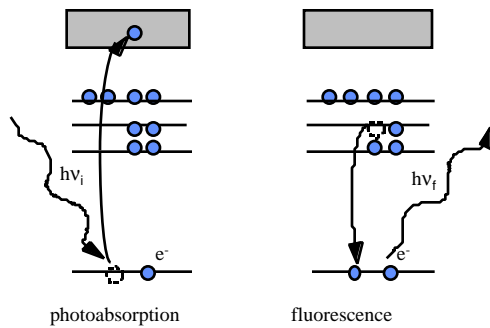


Fig. 6 Schematic of x-ray photoabsorption followed by fluorescence. An x-ray photon of energy  $h\nu_i$  is absorbed by the atom which ejects an electron from an inner shell of the atom. The atom fills the electron hole by emitting an x-ray with an energy  $h\nu_f$ ;  $h\nu_f$  is characteristic to the atom and has an energy equal to the energy difference between the initial and final hole-state energies. Alternatively the atom fills the inner-shell hole by emitting an energetic electron (Auger effect [Bambynek, et al., 1992]).

Photoabsorption and Compton scattering are best understood in terms of a particle-like interaction between x rays and matter (Fig. 6). The quantized energy of an x-ray photon excites an electron from a bound state to an unbound (continuum) state, while the photon momentum is transferred either to the atomic nucleus (Photoeffect) or to the electron (Compton scattering). X-ray fluorescence is the name given to the elementally distinct or “characteristic” x-ray spectra which is emitted from an atom as an inner shell hole is filled.

**Fluorescence yields.** An inner shell hole can also be filled by a non-radiative mechanisms (Auger and Coster-Kronig effects [Bambynek, et al., 1992]). Here the singly ionized atom fills the inner shell hole with a higher-energy electron and emits an energetic (Auger/Coster-Kronig) electron with a characteristic energy which is determined by the initial and final energy of the atom. The fraction of holes which are filled by x-ray fluorescence decay is referred to as the fluorescence yield. In general *non*-radiative processes become increasingly likely as the initial-hole binding energy decreases (Fig. 7). We note that for K holes with binding energies above 5 keV, the x-ray fluorescence yields are more than 20%. For L holes with binding energies greater than 5 keV, all fluorescence yields exceed

10%. The fluorescence yields of deep inner shell holes can exceed 90%.

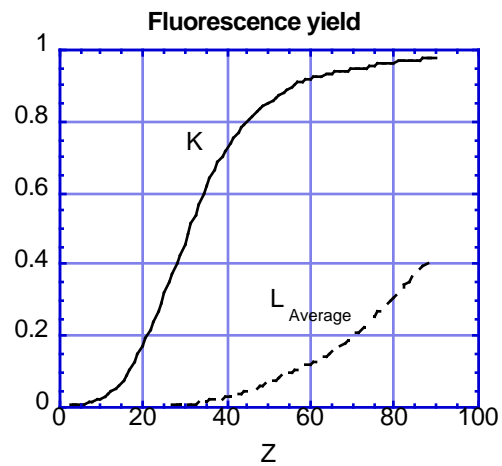


Fig. 7 Fit to experimental fluorescence yields for K and L holes (X-ray Absorption...,1998).

**Characteristic radiation.** The characteristic x-ray energies emitted when the initial hole decays by fluorescence serve as a “fingerprint” for the element and are quite distinct. Fluorescence spectra are labeled according to the electron hole being filled and the strength of the decay channel. For example as shown in Fig. 8,  $K\alpha_1$  fluorescence arises when an  $L_{III}$  ( $2P_{3/2}$ ) electron fills a K hole. This transition is the strongest fluorescence decay channel for K holes. A similar nomenclature is used for L holes, etc.

Because chemical effects on inner shell wavefunctions are small, x-ray absorption cross-sections, fluorescence yields, and characteristic x-ray spectra are virtually unchanged by sample environment except very near threshold. However, the measured-fluorescence signal *can* strongly depend on absorption and secondary excitation due to the sample matrix.

A typical spectra from a low Z matrix with trace elements is shown in Fig. 9. The characteristic lines have a natural bandwidth of a few eV which is smeared by the energy resolution of the detector. Even in this case where the trace elements are nearby in the periodic table, the fluorescence signature of each element is distinct. Crystal spectrometers with higher energy resolution can be used in more complicated cases

with overlapping L lines to resolve nearby fluorescence lines.

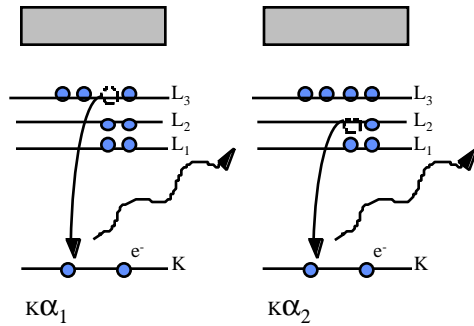


Fig. 8 Fluorescence decay channels for K holes.

Photoabsorption cross sections. To a first approximation only x-rays with sufficient energy to excite an electron above the Fermi level (above the occupied electron states) can create an inner shell hole. As a consequence, the photoabsorption cross-section for x rays has thresholds which correspond to the energy needed to excite an inner shell electron into unoccupied states. As shown in Fig. 10 the photoabsorption cross section exhibits a characteristic saw-tooth pattern as a function of x-ray energy. Highest x-ray efficiency for the creation of a given hole is just above its absorption edge energy. Maximum elemental sensitivity with minimum background results when the x-ray microprobe energy is tuned just above the absorption edge of the element of interest (Sparks, 1980). Because x rays are highly efficient at creating inner shell holes, x-ray excited fluorescence has very high signal-to-noise (Fig. 3) and the energy deposited in the sample is low for a given signal.

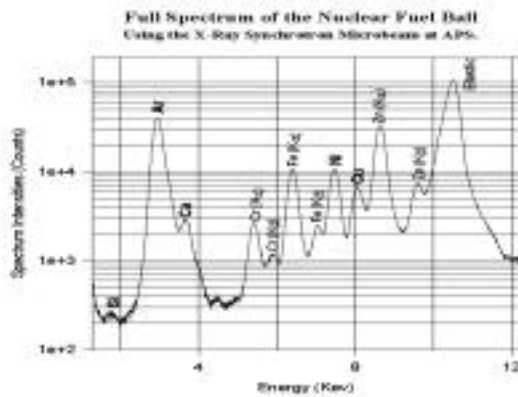


Fig. 9 Fluorescence spectra from the SiC shell of an advanced nuclear fuel particle. The trace

elements in the sample emit characteristic x-ray lines when excited with x rays.

Micro-XAFS. The saw tooth pattern of Fig. 10 shows the typical energy dependence of x-ray absorption cross sections over a wide energy range, but does not include life-time broadening of the inner shell hole, the density of unfilled electron states near the Fermi energy, or the influence of photoelectron backscattering. These various processes lead to fine structure in the photoabsorption cross section which can be used to determine the valence state of an element, its local neighbor coordination, and bond distances. Near edge absorption fine structure (NEXAFS) is particularly sensitive to the valence of the atom. Extended x-ray absorption fine structure (EXAFS) is sensitive to the near-neighbor coordination and bond distance. Fluorescence measurements have the best signal-to-background for XAFS of trace elements. It is therefore possible to use XAFS techniques with an x-ray microprobe to determine additional information about the local environment of elements within the probe region. More detail about XAFS techniques is given in unit 11.19 (X-Ray Absorption..., 1998).

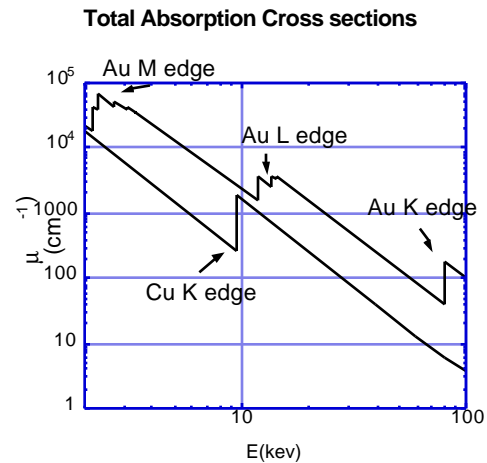


Fig. 10 Photoabsorption cross section for Cu and Au.

Penetration depth. The effective penetration depth of a fluorescence microprobe depends on the energy of the incident and fluorescent x-rays, the composition of the sample and the geometry of the measurement. As shown in Figs. 1 and 10, x-ray absorption decreases with an  $\sim E^{-3}$  power dependence between absorption edges. For a low Z matrix the penetration depth of an x-ray

microfluorescence beam can be tens of mm into the sample while for a high Z matrix the penetration can be only a few microns (Fig. 1).

With a thick sample, the fluorescence signal and effective depth probed depends on the total scattering angle and on the asymmetry of the incident to exit beam angles (Sparks, 1980). To a first approximation, the fluorescence signal is independent of total scattering angle but depends on the asymmetry between the incident angle  $\psi$  and the exit angle  $\phi$  (Fig. 11).

$$C_Z \propto \left( \mu_i + \mu_f \frac{\sin \psi}{\sin \phi} \right) \quad (2)$$

Here  $\mu_i$  is the linear absorption coefficient for the incident beam and  $\mu_f$  is the total absorption coefficient for the fluorescence beam. The approximation of Eq. 2 is only valid for uniformly smooth sample surfaces. Where sample granularity, and surface roughness are large the fluorescence signal decreases as the glancing angle decreases (Sparks, et al., 1992; Campbell, et al, 1985). The effective depth probed depends both on the total scattering angle  $\phi + \psi$ , and on the asymmetry between  $\psi$  and  $\phi$ .

The characteristic depth of an x-ray microprobe is given by,

$$x = \left( \frac{\mu}{\sin \psi} + \frac{\mu_f}{\sin \phi} \right)^{-1} \quad (3)$$

Shallow depth penetration can be achieved with glancing angle and asymmetric geometries. With smooth surfaces, even greater surface sensitivity can be achieved by approaching or achieving total external reflection from the surface (Brennan, et al., 1994). With total external reflection, the surface sensitivity can approach 1 nm (10 Å) or better (Fig. 12).

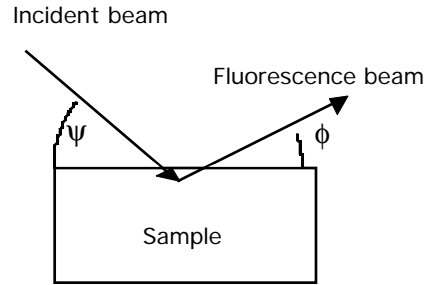


Fig. 11 Depth penetrated by a fluorescence microprobe depends on the total absorption cross section of the incident and fluorescence radiation and on the incident and exit angles with respect to the sample surface.

Backgrounds. Background signal is generated under fluorescence lines by various scattering and bremsstrahlung processes. With a white or broad bandpass incident beam, elastically scattered x rays of the same energy as the fluorescent line can be directly scattered into the detector. This scattering can be greatly reduced by operating at a  $2\theta$  scattering angle of  $90^\circ$  in the plane of the synchrotron where linear beam polarization inhibits elastic and Compton scattering. A much better way to reduce background is through the use of a monochromatic x-ray beam. As shown in Fig. 2, monochromatic x-ray beams produce the best signal-to-background because the background under a fluorescence peak must arise from multiple scattering events, bremsstrahlung from photoelectrons or other cascade processes.

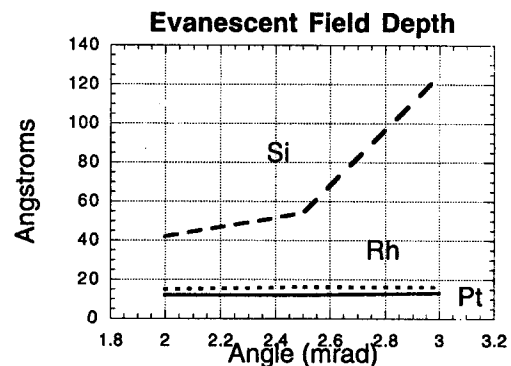


Fig. 12 Evanescent wave depth of 10 keV X-rays into Si Rh or Pt as a function of glancing angle.

Detectors. Two kinds of detectors are used for observing fluorescence. Solid-state detectors are

most widely used because they are efficient and can simultaneously detect many elements in the sample. A state-of-the-art solid state detector with a  $\text{cm}^2$  active area has about 130 eV resolution at 5.9 keV with a 5000 cps counting rate. Much higher counting rates are possible by compromising the energy resolution and by using multiple detector arrays. For example, 30 element arrays with 500,000 cps counting rates/element can achieve 15 million cps. One drawback with solid state detectors is additional background for trace elements which is introduced by high intensity peaks in the spectra. As shown in Fig. 13, a solid state detector typically has both short and long range low-energy tails due to insufficient charge collection (Cambell, 1990). These can be the dominant contribution to background under a trace element.

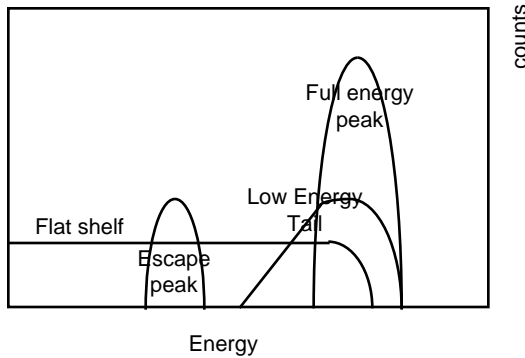


Fig. 13 Schematic of low-energy tails in a solid state detector.

Wavelength dispersive spectrometers can also be used to measure fluorescence.<sup>35-37</sup> These detectors have much poorer collection efficiency but much better energy resolution (lower background) and are not paralyzed by scattering or by fluorescence from the major elements in the sample. Because wavelength detectors only count one fluorescent energy at a time, they are not count-rate limited by fluorescence or scattering from the major elements in the sample matrix.

### X-ray Microdiffraction Analysis

X-ray microdiffraction is sensitive to phase (crystal structure), texture (crystal orientation), and strain (unit cell distortion) (Rebonato, et al., 1989; Ice, 1987). Diffraction (Fig. 14) is best understood in terms of the wave-like nature of x rays. Constructive and destructive interference

from x-ray scattering off the charge-density distribution varies the x-ray scattering efficiency as a function of angle and wavelength. This so called diffraction pattern can be Fourier transformed to recover charge density information. Although the basic diffraction process is identical for all diffraction probes (e.g. x rays, electrons, neutrons, etc.), x rays have three very favorable attributes for the characterization of crystal structure; (1) the wavelength is similar to the atomic spacing of matter; (2) the cross section is sufficiently low that multiple scattering effects are often small; and (3) the cross section of elastic scattering is a large fraction of the total interaction cross section of x rays which contributes to low noise. In addition, x-ray scattering contrast can be adjusted by tuning near to x-ray absorption edges (Materlik, et al., 1994).

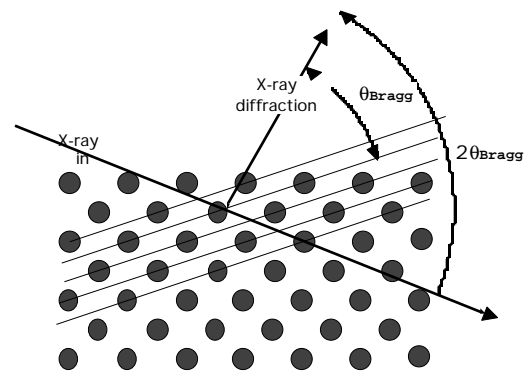


Fig. 14 X-ray diffraction from a crystal becomes large at Bragg angles where the crystal lattice spacing  $d$ , the wavelength  $\lambda$  and the angle of the incident beam with respect to the crystal lattice planes  $\theta_{\text{Bragg}}$  satisfy Bragg's law.

Strong diffraction occurs when the incident beam satisfies Bragg's Law,

$$2d \sin \theta = n\lambda \quad (4)$$

Here  $d$  is a crystal lattice spacing,  $\lambda$  is the x-ray wavelength, and  $\theta$  is the so called "Bragg angle" between the incident beam and the crystal plane. X-ray microdiffraction can yield detailed information about the sample unit cell and its orientation. If the x-ray wavelength is known, the angle between the incident and an intense exit beam ( $2\theta$ ) determine the spacing  $d$ . The relative orientation of crystals (mosaic spread or texture) can be determined by observing the rotation

angles of a sample needed to maximize scattered intensity. These two methods are useful for studies where there is strong preferred orientation.

For unknown crystal orientation, the unit-cell parameters and crystallographic orientation of a single crystal can be determined from the x-ray energy and the angles of three non-colinear reflections (Busing & Levy, 1967). In standard crystallography, reflections are found by rotation of the sample under the beam. With *microdiffraction* x-ray measurements on polycrystalline samples, however, the imprecision of mechanical rotations will cause the sample to translate relative to the beam on a micron scale. In addition, for complex samples with many crystals, the penetration of the x-ray beam into the specimen ensures that the sample volume (and therefore microstructure) will vary as the sample rotates (Fig. 15.). The changing grain illumination makes a standard crystallographic solution impossible. These two problems can be overcome by the use of Laue diffraction with white or broad-bandpass x-ray beams. With Laue diffraction no sample rotations are required. Development is in progress to automatically index the overlapping reflections of up to 10 crystals (Chung, 1997; Marcus, et al., 1996; and Wenk, et al., 1997).

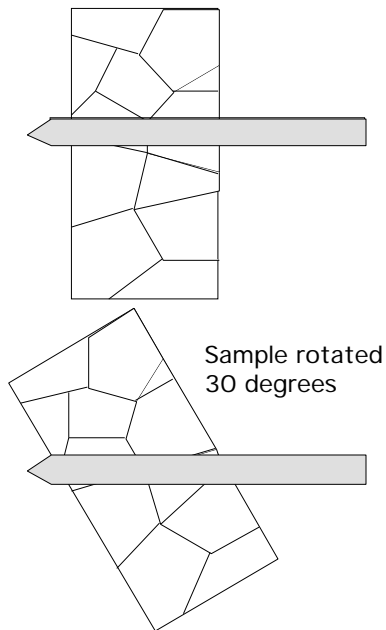


Fig. 15 The volume of a sample which is illuminated by a penetrating x-ray beam changes as the sample is rotated.

X-ray microdiffraction also allows for 3-D imaging of crystal structure as demonstrated in some first experiments (Stock, et al., 1995). For these measurements the sample to detector distance is changed and the origin of the reflecting crystal along the microprobe beam is determined by ray tracing (Fig. 16).

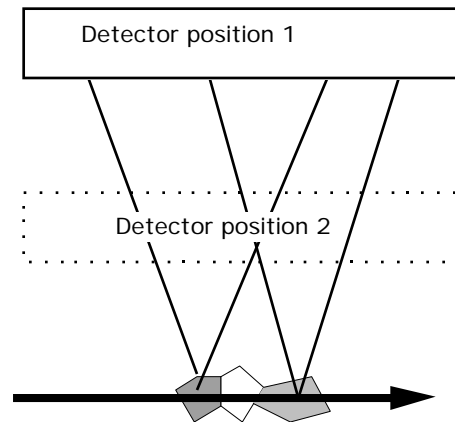


Fig. 16. Three-dimensional imaging of sample crystallography by triangulation.

## PRACTICAL ASPECTS OF THE METHOD

### Sources

Only second- and third-generation synchrotron sources have sufficient x-ray brilliance for practical x-ray microprobe instrumentation. World-wide there are only three third-generation sources suitable for hard x-ray microprobes: the 6 GeV European Synchrotron Radiation Facility in Grenoble France<sup>10</sup>, the 7 GeV Advanced Photon Source at Argonne, Illinois<sup>11</sup>, USA, and the 8 GeV Spring-8 under construction in Japan. Although third generation sources are preferred, x-ray microprobe work can also be done on second generation sources like the National Synchrotron Light Source (NSLS) Brookhaven, New York. A world-wide map of synchrotron radiation facilities with x-ray microbeam instrumentation is shown in Fig.17. A list of contacts is given in Table 2.

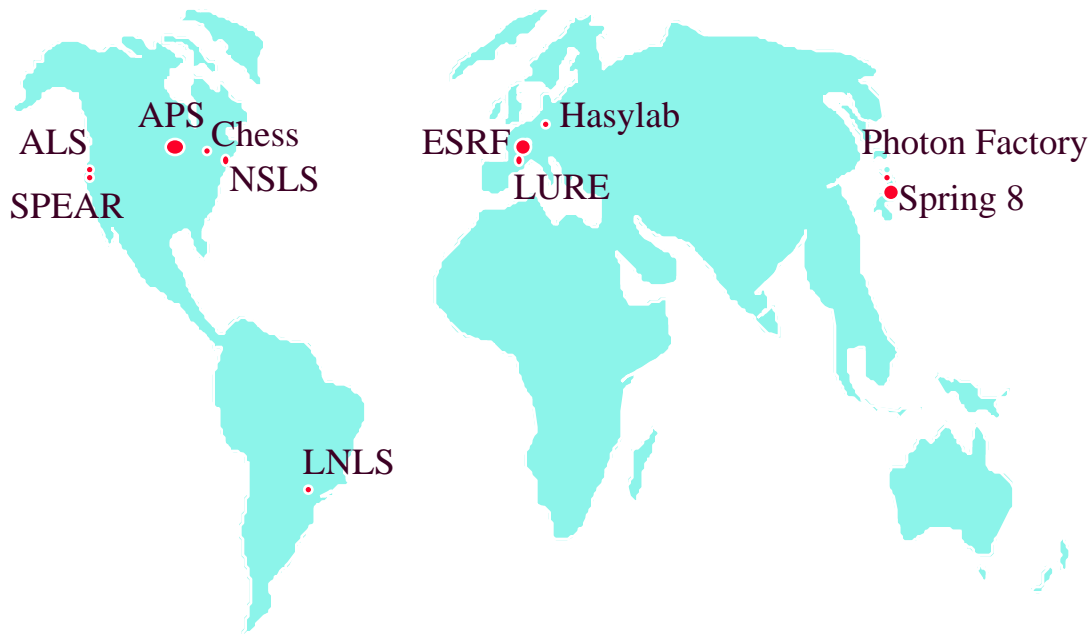


Fig. 17 Geographic distribution of synchrotron sources with hard x-ray microprobe instrumentation.

Table 2. World-Wide dedicated x-ray microbeam facilities. The top four facilities are on hard x-ray third-generation sources. The ALS x-ray microprobe is on a third generation VUV ring with a small emittance beam which acts like a high-performance second generation ring for hard x-rays. The remaining beamlines are on second generation rings.

Facility	Beamline	hν (keV)	Spot size $\mu\text{m}^2$	$\Delta E/E$	Total Flux (photons/s)	Local Contact	Email
APS	2-ID-CD	5-20	~ 1	$2 \times 10^{-4}$	$1 \times 10^{11}$	Wen-Bing Yun	Yun@aps.anl.gov
APS	ID-13	5-25	~25	$2 \times 10^{-4}$	$1 \times 10^{13}$	Steve Sutton	Sutton@cars.uchicago.edu
ESRF	ID-13	6-16	~40	$2 \times 10^{-4}$	$2 \times 10^{11}$	Christian Riekkel	riekkel@esrf.fr
ESRF	ID-22	4-35	~ 2	$2 \times 10^{-4}$	$10^9$ - $10^{12}$	Anatoly Snigirev	snigirev@esrf.fr
ALS	10.3.1	6-12	~ 2	$5 \times 10^{-2}$	$2 \times 10^{10}$	Scott McHugo	samchugo@lbl.gov
LNLN		2-14	100	$2 \times 10^{-4}$ white	$3 \times 10^7$ $3 \times 10^9$	Helio C.N. Tolentino	helio@lnln.br
CHESS	B2	5-25	0.001	$2 \times 10^{-2}$	$10^6$	Don Bilderbach	dhb2@cornell.edu
Photon Factory	BL4-A	5-15	25	$2 \times 10^{-4}$ $5 \times 10^{-2}$	$10^8$ $10^{10}$	A. Iida	
Hasylab	L	4-80	9			Thomas Wroblewski	wroblewt@mail.desy.de
Hasylab	BW-1	10	1	$1 \times 10^{-2}$	$6 \times 10^7$	Thomas Wroblewski	wroblewt@mail.desy.de
DCI LURE	D15	6,10, 14	~1-100	$2 \times 10^{-2}$	$10^5$ - $10^7$	P. Chevallier	chevallier@lure.u-psud.fr
SSRL						J. Patel	Patel@ssrl01.Slac.stanford.edu
NSLS	X16C	5-20	$4 \mu\text{m}^2$	White	$10^{10}$	M. Marcus	
NSLS	X26A	5-20	~10- $200 \mu\text{m}^2$	$10^{-4}$ white	$7 \times 10^7$ - $7 \times 10^{10}$	Steve Sutton	Sutton@cars.uchicago.edu

## Optics

**Tapered capillaries.** The development of intense synchrotron x-ray sources, with at least 11 orders of magnitude greater brilliance than conventional x-ray sources (Fig. 2), has revived interest in x-ray optics. At least three microbeam forming options have emerged with various strengths and weaknesses for experiments.<sup>12</sup> Tapered capillary optics (Fig. 18) have produced the smallest x-ray beams (Stern, et al., 1988; Larsson & Engström, 1992; Hoffman, et al., 1994). Bilderbach, et al. (1994) have reported beams as small as 50 nm FWHM. This option appears to be the best for condensing beams below 0.1 $\mu$ m. One concern with capillary optics, however, is their effect on beam brilliance. Ray tracing and experimental measurements have found that the angular divergence following a capillary has a complex annular distribution. This distribution arises from roughness inside the capillary and from the non-equal number of reflections of different rays as they are propagated along the capillary.

### Tapered Capillary

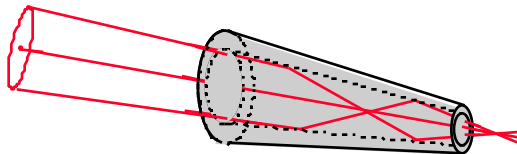


Fig. 18 Schematic of a tapered capillary condensing element.

**Zone plates.** Hard x-ray zone plates (Fig. 19) are a rapidly emerging option for focusing synchrotron radiation to  $\mu$ m dimensions (Yun, et al., 1992; Bionta, et al., 1990). This option appears especially promising for focusing monochromatic radiation ( $\Delta E/E \sim 10^{-4}$ ). These devices are simple to align, allow good working distance between the optics and the sample, and have already achieved sub micron spots. Although zone plates are inherently chromatic, they can in principle be used with tunable radiation by a careful translation along the beam direction. State-of-the-art zone plates provide the most convenient optics for monochromatic experiments even though their focusing efficiency has not reached the 40-60% efficiency promised by more advanced designs.

### Fresnel Zone Plate

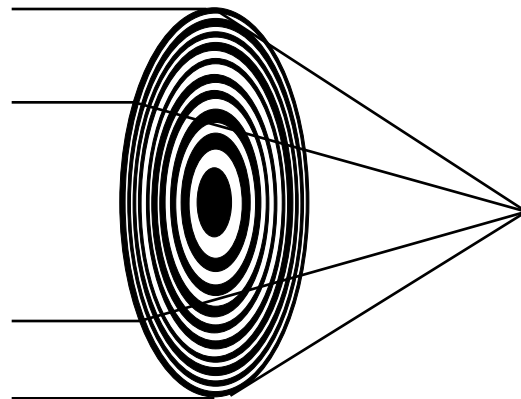


Fig. 19 Hard x-ray zone plate for focusing synchrotron radiation.

**Kirkpatrick-Baez Mirrors.** Kirkpatrick-Baez (KB) mirrors provide a third highly promising option for focusing synchrotron radiation (Underwood, et al., 1996; Yang, et al., 1995). A Kirkpatrick-Baez mirror pair consists of mirrors which condense the beam in orthogonal directions (Fig. 20). Both multilayer and total-external-reflection mirrors have been used for focusing synchrotron radiation. Multilayer mirrors appear most suitable for fluorescence measurements with a fixed wide-bandpass beam and where large divergences can be accepted. Total-external-reflection mirrors appear to offer the best option for focusing white beams to  $\mu$ m dimensions. The key challenge with KB mirrors is achieving low figure and surface roughness with elliptical surfaces. There are numerous parallel efforts currently underway to advance mirror figuring for advanced KB focusing schemes.

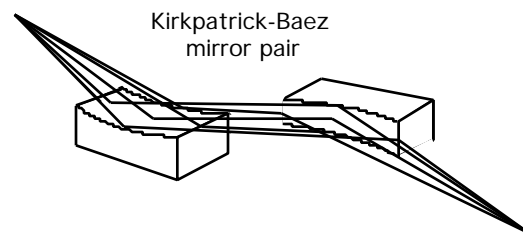


Fig. 20 Schematic of a two-mirror Kirkpatrick-Baez pair.

**Refractive Lenses.** In addition to the focusing schemes mentioned above, there are two new options which have recently emerged from experiments at the European Synchrotron Radiation Facility (ESRF). These are compound refractive lenses (Fig. 21) and Bragg Fresnel optics (Fig. 22). Compound refractive lenses are very interesting because they are relatively easy to manufacture (Snigirev, et al., 1996). Estimates of their theoretical efficiency, however, indicate that they cannot compete with the theoretical efficiency of KB mirrors or zone plates.

**Compound refractive lens**

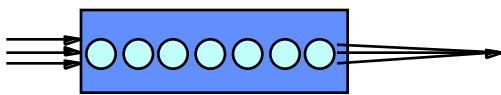


Fig. 21 X-ray compound refractive lens.

**Bragg Fresnel Lens**

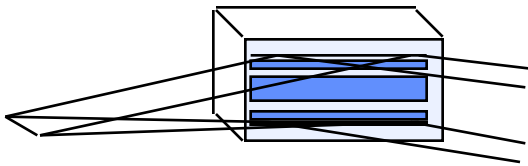


Fig. 22 Bragg Fresnel lens.

**Bragg-Fresnel Optics** Bragg-Fresnel optics are also an interesting option used both at LURE and the ESRF (Aristov, 1988). With Bragg-Fresnel optics, the phase contrast steps are lithographically etched into a multilayer or monolithic Si substrate. This offers a rugged coolable substrate and serves to simultaneously focus and monochromatize the beam. Some of the alignment simplicity of zone plates is lost with these devices because the beam is deflected, but they have the advantage that the 0th order (direct beam) is spatially removed from the focus and can therefore be easily stopped.

**MICROBEAM APPLICATIONS**

Microprobe analysis has already been applied to many problems with second and third generation x-ray beams (Rebonato, et al., 1989; Langevelde, et al., 1990; Thompson, et al., 1992; Jones & Gordon, 1989; Wang, et al., 1997). Studies include measurement of strain and texture in integrated circuit conduction paths

(Wang, et al., 1997), the measurement of buried trace elements in dissolution reactions (Perry & Thompson, 1994), and determination of chemistry in small regions. Three simple examples are given to illustrate possible applications.

**Example 1: Trace element distribution in a SiC nuclear fuel barrier.**

TRISO coated fuel particles contain a small kernel of nuclear fuel encapsulated by alternating layers of C and SiC as shown in Fig. 23. The TRISO coated fuel particle is used in an advanced nuclear fuel designed for passive containment of the radioactive isotopes. The SiC layer provides the primary barrier for radioactive elements in the kernel. The effectiveness of this barrier layer under adverse conditions is critical to containment.



Fig. 23 Schematic of TRISO fuel element.

Shell coatings were evaluated to study the distribution and transport of trace elements in the SiC barrier after being subjected to various neutron fluences (Naghedolfeizi, et al., 1998). The C buffer layers and nuclear kernels of the coated fuel were removed by laser drilling through the SiC and then leeching the particle in acid (Myers, et al., 1986). Simple x ray fluorescence analysis can detect the presence of trace elements but does not indicate their distribution. Trace elements in the SiC are believed to arise at least in part as daughter products from the fission process; lower trace elements concentrations are found in un-irradiated samples. The radial distribution of these elements in the SiC shells can be attributed to diffusion of

elements in the kernel due to thermal and radiation enhanced diffusion. Other elements in the shells may originate in the fabrication of the TRISO particles.

Linear x-ray microprobe scans were made through the SiC shell. X-ray fluorescence is an ideal tool for this work because it is nondestructive (no spread of contamination), it is sensitive to heavy elements in a low Z matrix, and because it provides a picture of the elemental distribution. Results of a simple line scan through a leached shell are shown in Fig.24. This scan was made with 2 $\mu$ m steps and an  $\sim$ 1  $\mu$ m probe. As seen in Fig. 24, very localized Fe rich regions less than 1  $\mu$ m broad are observed throughout the shell. This behavior is typical of other trace elements observed in the shell.

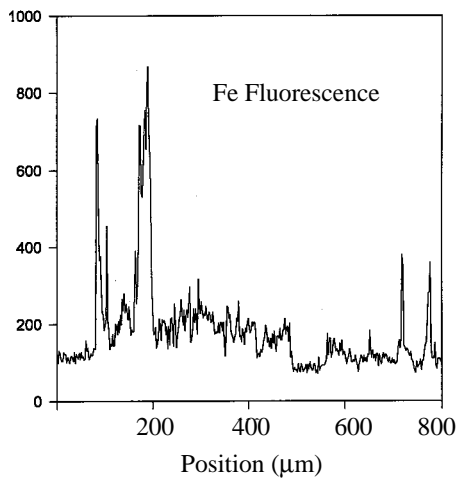


Fig. 24 The Fe fluorescence during a line scan through a SiC shell shows a complicated spatial distribution with sharp features less than 1 $\mu$ m wide.

The spatial distribution can be further investigated by extending the x-ray microprobe analysis to x-ray microfluorescence tomography (Naghedolfeizi, et al., 1998; Biosseau, 1986). Although x-ray fluorescence tomography is inherently time consuming, the method yields three-dimensional distributions of trace elements. For example, the Zn distribution in a plane of the SiC shell is illustrated in Fig. 25.

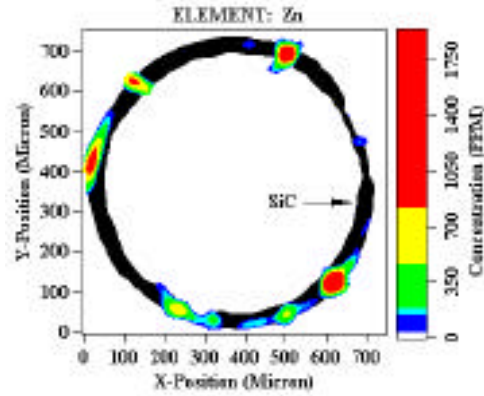


Fig. 25 Zn distribution in a SiC shell after reconstruction from x-ray microfluorescence data (reference 59). The spatial resolution was limited because time restricted the number of steps.

### Example 2: Change in the strain distribution near a notch during tensile loading.

Early experiments with second generation sources demonstrated some of the features of x-ray microprobe based diffraction: good strain resolution, ability to study strain in thick samples, ability to study dynamics of highly strained samples, and the ability to distinguish lattice dilation from lattice rotations. For example, a measurement of differential strain induced by pulling on a notched Mo single crystal (Rebonato, et al., 1989) shows lattice dilation above the notch and a lattice contraction below the notch (Fig. 26). This behavior would be totally masked with a topographic measurement because of the high density of initial dislocations. In addition, the measurement allowed the lattice rotations to be separated from the lattice dilations. Finally, the measurements are quantitative, and even in this early experiment yielded strain sensitivity  $\Delta d/d$  of  $\sim 5 \times 10^{-4}$ .

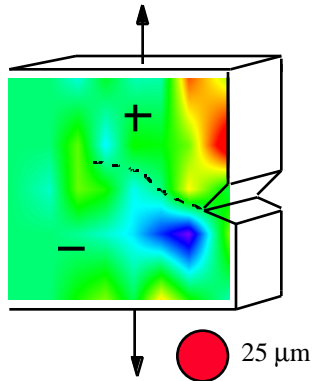


Fig. 26 Strain map in a Mo single crystal from reference 2 showing  $\Delta d/d$  for the (211) planes when the crystal is pulled. A region of contraction (below the dashed line) and a region of elongation (above the dashed line) are observed. The reduction in  $d$  beneath the dashed line arises from the orientation of the observed Bragg plane with respect to the free surface. The probe size of  $\sim 25\mu\text{m}$  was barely small enough to detect the strain features.

### Example 3: Strain distribution in an advanced ferroelectric sample.

$\text{BaTiO}_3$  has a tetragonal structure in the ferroelectric state. For a single crystal thin film deposited on Si, the tetragonal axis can lie either in the plane of the thin film or normal to the surface. The direction of the tetragonal axis is referred to as the “poled” direction. It is of great technical importance to understand the distribution of poled regions in advanced ferroelectric  $\text{BaTiO}_3$  films on semiconductor substrates. X-ray microdiffraction has been used to study the spatial distribution of poling with  $\sim 1 \times 10 \mu\text{m}^2$  spatial resolution. In the experiment, an x-ray microbeam was directed onto various regions of the  $\text{BaTiO}_3$  film. The diffraction pattern from the film was recorded on a CCD x-ray detector.

A typical diffraction pattern shown in Fig. 27 illustrates many of the powerful attributes of microdiffraction. The  $\text{BaTiO}_3$  002/200 Bragg peak appears as a lenticular intense pattern in the CCD image even though it is covered with a 200 nm cap of aluminum. The strain in the thin film can be measured to  $\Delta d/d \sim 1 \times 10^{-5}$ . This is sufficient to easily resolve the  $\sim 1\%$  difference in the lattice parameter between 002 or 200 poled  $\text{BaTiO}_3$ . Texture, particle size, and strain of the powder-like aluminum overlayer can be inferred directly from the 111 and 200 Debye rings as

seen in the lower part of Fig. 27. Even better strain resolution can be obtained by measurement of higher order reflections.

This example clearly indicates the need for an x-ray diffraction microprobe. Small spot size is required to study the distribution of poled material near small dimensioned features of the film. Good strain resolution is required to differentiate between the various poling options. A penetrating probe is required to measure the film in an unaltered state below a 200 nm cap of aluminum.

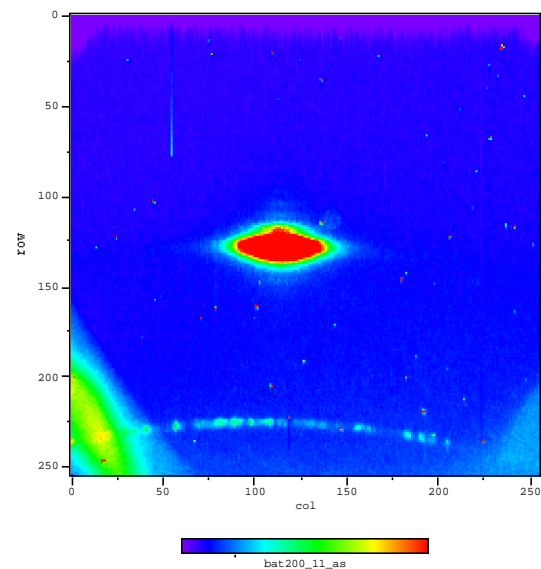


Fig. 27 X-ray microdiffraction image from an advanced thin film. The CCD image shows the single crystal reflection and the powder-like image from the Al overlayer.

## METHOD AUTOMATION

X-ray microfluorescence and x-ray microdiffraction data collection at synchrotrons occurs remotely in a hostile high radiation environment. Experiments are located inside shielded hutches which protect the researcher from the x rays near the experiment but which restrict “hands on” manipulation of the experiment. Fluorescence and simple diffraction measurements are typically made by step-scanning the sample under the beam. A record is made of fluorescence spectrum or the diffraction pattern from the sample at hundreds to thousands of positions.

Efforts are now underway to further automate the data collection of both microfluorescence and microdiffraction analysis. To avoid the storage of huge data files, fluorescence spectra are often stored as “regions of interest.” This procedure works well in many cases, but can lose important information for overlapping characteristic lines. A better solution is to record complete spectra or to fit the spectra on the fly to separate overlapping peaks.

With microdiffraction experiments a key challenge is automated indexing of Laue reflections. This quite general problem appears feasible for wide bandpass x-ray beams  $\Delta E/E \sim 5-10\%$  and for samples where the unit cell is known (but not the orientation or strain) (Chung, 1997; Marcus, et al., 1996; Wenk, et al., 1997).

## **DATA ANALYSIS AND INITIAL INTERPRETATION**

For many samples, x-ray microfluorescence and x-ray micro-diffraction can yield rather direct information about trace element and crystal texture/strain distributions. X-ray fluorescence data can be placed on an absolute scale if the approximate composition of the sample is understood and the incident flux known. Because of uncertainties in the absorption coefficients of x rays, first principles methods are only good to about 5% (Sparks, 1980; Lachance & Claisse, 1995). More precise absolute measurements can be obtained with prepared standards.

For inhomogeneous samples however, variations in thickness, sample density and geometry can complicate data analysis. For example surface roughness, inhomogeneous absorption, variations in secondary fluorescence and other inhomogeneous matrix effects can drastically complicate absolute data analysis.<sup>62</sup>

With a monochromatic x-ray beam, relative texture and strain information can be obtained rather directly from measured microdiffraction angles. However again standards are useful to put strain and orientation information on an absolute scale.

## **SAMPLE PREPARATION**

One of the major advantages of x-ray microprobe analysis is the minimal sample preparation. In general, samples need to be small due to the short working distances between the focusing optics and the focus. Samples should be mounted on low background materials to reduce x-ray scatter and fluorescence.

Because of the sensitivity of x-ray microfluorescence to trace elements, particular care must be taken during sample mounting to prevent contamination of the sample. For example, samples should be handled with low-Z plastic tweezers to avoid metal contamination from metallic tweezers.

To aid in sample throughput, some microbeam instrumentation has been designed with mounting systems which allow the sample to be mounted on an optical microscope remote from the x-ray microprobe. The position of the sample with respect to a fiducial in the remote microscope holder can be accurately reproduced on the x-ray microbeam positioning stage. Features of interest can be identified off line and their co-ordinates noted for later x-ray microcharacterization.

## **PROBLEMS**

As described previously, the two key problems of x-ray microbeam analysis are the limited number of useful sources and the difficulty of fabricating efficient x-ray optics. In addition to these two problems there are several annoying problems which complicate the use of x-ray microbeam techniques. One difficulty with x-ray microbeam experiments is identification of the x-ray beam position on the sample. Because of the small beam size, even intense x-ray microbeams are difficult to view on fluorescent screens with visible light optics and even when they are visualized the transfer from beam position on a fluorescence screen to beam position on a sample can be difficult. For some experiments it is necessary to place markers on the sample to help in locating the x-ray beam. For example, a cross-hair of a fluorescing heavy metal can be used to locate the beam position with respect to an interesting region.

Another annoying problem with x-ray microbeam analysis is the difficulty of monitoring the absolute beam intensity on the sample. Because the distance from the focusing optics to the focus is typically short, there is little room to install a transmission beam monitor. Even when such a monitor is installed, great care must be taken to avoid contamination of the monitor signal due to backscatter from the sample.

The problem of backscatter contamination into a transmission monitor is but one example of a general class of shielding problems which arise

due to the proximity of sample, detector and optics. In general great care is required to reduce parasitic backgrounds associated with the beam path through x-ray optics and any air path to the sample. Typically scatter from beam defining slits and upstream condensing optics can swamp a CCD detector unless care is taken to shield against such direct scattering. The short working distance between the optics and the sample also require care to avoid collisions.

## LITERATURE CITED

- Anderson, I. and Marienko, R. B. 1998. Electron probe microanalysis. *Methods in Materials Research* 12c.1.
- Aristov, V. V. 1988. X-ray Microscopy II p. 108-117; Chevallier, P., Dhez, P., Legrand, F., Idir, M., Soullie, G., Mirone, A., Erko, A., Snigirev, A., Snigireva, I., Suvorov, A., Freund, A., Engstrom, P., Als. Nielsen, J., and Grubel, A., 1995. Microprobe with Bragg-Fresnel multilayer lens at ESRF beam line. *NIM A* 354:584-587; Snigirev, A., Snigireva, I., Bosecke, P., Lequien, S., and Schelokov, I. 1997. High energy X-ray phase contrast microscopy using a circular Bragg-Fresnel lens. *Optic Comm.* 135:378-384.
- Bambynek, W., Crasemann, B., Fink, R. W., Freund, H. U., Mark, H., Swift, C. D., Price, R. E., and Venugopala Rao, P. 1992. X-ray Fluorescence Yields, Auger and Coster-Kronig Transition Probabilities. *Rev. Mod. Phys.* 44:716-813.
- Banks, J. C. and Knapp, J. A. 1998. Heavy ion backscattering spectrometry. *Methods in Materials Research* 13c.2.
- Bilderback, D. H., Hoffman, S. A., and Thiel, D. J. 1994. Nanometer spatial resolution achieved in hard X-ray imaging and Laue diffraction experiments. *Science* 263:201-202.
- Bionta, R. M., Ables, E., Clamp, O., Edwards, O. D., Gabriele, P. C., Miller, K., Ott, L. L., Skulina, K. M., Tilley, R., and Viada, T. 1990. Tabletop X-ray microscope using 8 keV zone plates. *Opt. Eng.* 29:576-580.
- Boisseau, P. 1986. Determination of three dimensional trace element distributions by the use of monochromatic X-ray microbeams. M.I.T. Ph.D. Dissertation.
- Brennan, S., Tompkins, W., Takaura, N., Pianetta, P., Laderman, S. S., Fischer-Colbrie, A., Kortright, J. B., Madden, M. C., and Wherry, D. C. 1994. Wide band-pass approaches to total-reflection X-ray fluorescence using synchrotron radiation. *Nucl. Instr. and Meth. A* 347:417-421.
- Buras, B. and Tazzari, S. 1984. European Synchrotron Radiation Facility Report of European Synchrotron Radiation Project. Cern LEP Div., Geneva, Switzerland.
- Busing, W. R. and Levy, H. A. 1967. Angle calculations for 3- and 4-circle X-ray and neutron diffractometers. *Acta Cryst.* 22:457-464.
- Cambell, J. L. 1990. X-ray spectrometers for PIXE. *Nucl. Instr. and Meth. B* 49:115-125.
- Campbell, I. and Guelph, U. 1998. Proton induced X-ray emission. *Methods in Materials Research* 13b.3.
- Campbell, J. R., Lamb, R. D., Leigh, R. G., Nickel, B. G., and Cookson, J. A. 1985. Effects of random surface roughness in PIXE analysis of thick targets. *Nucl. Instr. and Meth. B* 12:402-412; Orlic, I., Van Langevelde, F., and Vis, R. D. 1990. The influence of sample roughness on the quantification of micro-PIXE results. *Nucl. Instr. and Meth. B* 49:74-77.
- Chevallier, P. and Dhez, P. 1997. Hard X-ray Microbeam: Production and Application. *In Accelerator based atomic physics techniques and applications* (S.M. Shafroth and J. Austin, eds.) pp. 309-348 AIP Press, New York.

- Chung, J.-S. 1997. Automated indexing of wide-band-pass Laue images. 1997 APS Users Meeting Workshop on Making and Using Very Small X-ray Beams. APS. Argonne II; Chung, J.-S. and Ice, G. E. 1998. Automated indexing of Laue images from polycrystalline materials. MRS Spring Symposium, San Francisco, CA.
- Cowley, J. and Marks, L. D. 1998. Reflection high energy electron diffraction. *Methods in Materials Research* 12c.2.
- Doyle, B. L., Walsh, D. S., and Lee, S. R. 1991. External micro-ion-beam analysis (X-MIBA). *Nucl. Inst. and Meth. B* 54:244-257.
- Eades, J. A. 1998. Convergent beam electron diffraction. *Methods in Materials Research* 12c.3.
- Folkmann, F. and Frederiksen, F. 1990. High-resolution X-ray spectrometer for PIXE work. *Nucl. Inst. and Meth. B* 49:126-131.
- Goldstein, J. I. 1979. Principles of thin film x-ray microanalysis. In Introduction to Analytical electron Microscopy (J. J. Hern, J. I. Goldstein, and D. C. Joy, eds.) pp. 83-120. Plenum Press, New York.
- Hoffman, S. A., Thiel, D. J., and Bilderback, D. H. 1994. Applications of single tapered glass capillaries-submicron X-ray imaging and Laue diffraction. *Optical Engineering* 33:303-306; Thiel, D. J., Stern, E. A., Bilderback, D. H., and Lewis, A. 1989. Focusing of synchrotron radiation using tapered glass capillaries. *Physica B* 158:314-316.
- Howells, M. R. and Hastings, J. B. 1983. Design considerations for an X-ray microprobe. *Nucl. Inst. and Meth.* 208:379-386.
- Ice, G. E. 1997. Microbeam-forming methods for synchrotron radiation. *X-ray Spectrometry* 26:315-326.
- Ice, G. E. 1987. Microdiffraction with synchrotron radiation. *Nucl. Inst. and Meth. B* 24/25:397-399.
- Ice, G. E. and Sparks, Jr., C. J. 1984. Focusing optics for a synchrotron X-radiation microprobe. *Nucl. Inst. and Meth.* 222:121-127.
- Ice, G. E. and Sparks, C. J. 1991. MICROCAT proposal to APS.
- Jones, K. W. and Gordon, B. M. 1989. Trace element determinations with synchrotron-induced X-ray emission. *Anal. Chem.* 61:341A-356A.
- Joshi, A. 1998. Auger electron spectroscopy. *Methods in Materials Research* 12c.2:.
- Lachance, G. R. and Claisse, F. 1995. Quantitative X-ray Fluorescence Analysis: Theory and Application. J. Wiley and Sons, New York.
- Langevelde, F. V., Tros, G. H. J., Bowen, D. K., and Vis, R. D. 1990. The synchrotron radiation microprobe at the SRS, Daresbury (UK) and its applications. *Nucl. Inst. and Meth. B* 49:544-550; Hayakawa, S., Gohshi, Y., Iida, A., Aoki, S., and Ishikawa, M. 1990. X-ray microanalysis with energy tunable synchrotron x-rays. *Nucl. Inst. and Meth. B* 49:555; Chevallier, P., Dhez, P., Legrand, F., Irko, A., Agafonov, Y., Panchenko, L. A., and Yakshin, A. 1996. The LURE-IMT photon microprobe. *J. of Trace and Microprobe Techniques* 14:517-540.
- Larsson, S. and Engström, P. 1992. X-ray microbeam spectroscopy with the use of capillary optics. *Adv. in X-ray Analysis* 35:1019-1025.

- Lindh, U. 1990. Micron and submicron nuclear probes in biomedicine. *Nucl. Inst. and Meth. B* 49:451-464.
- Making and Using Very Small X-ray Beams. 1997 APS Users Meeting Workshop, Argonne Technical report.
- Marcus, M. A., MacDowell, A. A., Isaacs, E. D., Evans-Lutterodt, K., and Ice, G. E. 1996. Submicron resolution X-ray strain measurements on patterned films: Some hows and whys. *Mat. Res. Soc. Symp.* 428:545-556.
- Materlik, G., Sparks, C. J., and Fischer, K. 1994. Resonant Anomalous X-ray Scattering. North Holland, Amsterdam.
- Michael, J. R. and Goehner, R. P. 1993. Crystallographic phase identification in scanning electron microscope: backscattered electron Kikuchi Patterns imaged with a CCD-based detector. *MSA Bulletin* 23:168-175; Goyal, A., Specht, E. D., Wang, Z. L., and Kroeger, D. M. 1997. Grain boundary studies of high-temperature superconducting materials using electron backscatter Kikuchi diffraction. *Ultramicroscopy* 67:35-57; Wilkinson, A. J. 1997. Methods for determining elastic strains from electron backscattering diffraction and electron channeling patterns. *Mat. Sci. and Tech.* 13:79.
- Miller, M. K., A. Cerezo, Hetherington, M. G., and Smith, G. D. W. 1996. Atom Probe Field Ion Microscopy. Oxford Science Publications, Oxford, England.
- Myers, B. F., Montgomery, F. C., and Partain, K. E. 1986. The transport of fission products in SiC. Doc No. 909055, GA Technologies Inc.
- Naghdolfeizi, M., Chung, J.-S., and Ice, G. E. 1998. X-ray fluorescence microtomography on a SiC nuclear fuel ball. Submitted to *Spring Mat. Res. Soc. Symp.*
- Perry, D. L. and Thompson, A. C. 1994. Synchrotron induced X-ray fluorescence microprobe studies of the copper-lead Sulfide solution interface. *Am. Chem. S. Abstract* 208:429.
- Piotrowski, D. P., Stock, S. R., Guvenilir, A., Haase, J. D., and Rek, Z. U. 1996. High resolution synchrotron X-ray diffraction tomography of large-grained samples. *Mat. Res. Soc. Symp. Proc.* 437:125-128.
- Rebonato, R., Ice, G. E., Habenschuss, A., and Bilello, J. C. 1989. High-resolution microdiffraction study of notch-tip deformation in Mo single crystals using X-ray synchrotron radiation. *Phil. Mag A* 60:571-583.
- Ren, S. X., Kenik, E. A., Alexander, K. B., and Goyal, A. 1997. Exploring spatial resolution in electron back-scattered diffraction (EBSD) experiments via Monte Carlo simulation. Submitted to *Ultramicroscopy*.
- Riekkel, C. 1992. Beamline for microdiffraction and micro small-angle scattering. *SPIE* 1740:181-190; and Riekkel, C., Bosecke, P., and Sanchez del Rio, M. 1992. 2 High brilliance beamlines at the ESRF dedicated to microdiffraction, biological crystallography and small angle scattering. *Rev. Sci. Instrum.* 63:974-981.
- Samorjai, G. A. 1998. Low energy electron diffraction. *Methods in Materials Research* 12b.1.
- Shenoy, G. K., Viccaro, P. J., and Mills, D. M. 1988. Characteristics of the 7 GeV advanced photon source: A guide for users. ANL-88-9 Argonne National Laboratory, Argonne. II.

- Snigirev, A., Kohn, V., Snigireva, I., and Legeler, B. 1996. A compound refractive lens for focusing high-energy X-rays. *Nature* 384:49-51.
- Sparks, Jr., C.J. 1980. X-ray Fluorescence Microprobe for Chemical Analysis. *In Synchrotron Radiation Research* (H. Winick and S. Doniach, eds.) pp. 459-512. Plenum, New York 1980.
- Sparks, C. J., Kumar, R., Specht, E. D., Zschack, P., Ice, G. E., Shiraishi, T., and Hisatsune, K. 1992. Effect of powder sample granularity on fluorescent intensity and on thermal parameters in X-ray diffraction rietveld analysis. *Advances in X-ray Analysis* 35:57-62.
- Stern, E. A., Kalman, Z., Lewis, A., and Lieberman, K. 1988. Simple method for focusing X-rays using tapered capillaries. *Appl. Opt.* 27:5135-5139.
- Stock, S. R., Guvenilir, A., Piotrowski, D. P., and Rek, Z. U. 1995. High resolution synchrotron X-ray diffraction tomography of polycrystalline samples. *Mat. Res. Soc. Symp.* 375:275-280;
- Suortti, P., Pattison, P., and Weyrich, W. 1986. An X-ray spectrometer for inelastic scattering experiments. I. Curved-crystal X-ray optics. *J. Appl. Cryst.* 19:336-342.
- Thompson, A. C., Chapman, K. L., Ice, G. E., Sparks, C. J., Yun, W., Lai, B., Legnini, D., Vicarro, P. J., Rivers, M. L., Bilderback, D. H., and Thiel, D. J. 1992. Focusing optics for a synchrotron-based X-ray microprobe. *Nucl. Instr. and Meth. A* 319:320-325.
- Underwood, J. H., Thompson, A. C., Kortright, J. B., Chapman, K. C., and Lunt, D. 1996. Focusing x-rays to a 1  $\mu\text{m}$  spot using elastically bent, graded multilayer coated mirrors. *Rev. Sci. Instr. Abstract* 67: 3359.
- Veigele, W. J., Briggs, E., Bates, L., Henry, E. M., and Bracewell, B. 1969. X-ray Cross Section Compilation from 0.1 keV to 1 MeV. Kaman Sciences Corp. Report No. DNA 2433F.
- Venugopala Rao, P. 1975. Inner-Shell Transition Measurements with Radioactive Atoms. *In Atomic Inner-Shell Processes, Vol II.* (B. Crasemann, ed.) pp. 1-32. Academic Press, New York.
- Wang, P. C., Cargill III, G. S., Noyan, I. C., Liniger, E. G., Hu, C. K., and Lee, K. Y. 1997. Thermal and electromigration strain distributions in 10 $\mu\text{m}$ -wide aluminum conductor lines measured by x-ray microdiffraction. *Mat. Res. Soc. Symp. Proc.* 473:273; Wang, P. C., Cargill, G. S., Noyan, I. C., Liniger, E. G., Hu, C. K., and Lee, K. Y. 1996. X-ray microdiffraction for VLSI. *Mat. Res. Soc. Symp. Proc.* 427:35.
- Wenk, H. R., Heidelberg, F., Chadeigner, D., and Zontone, F. 1997. Laue orientation imaging. *J. Synchrotron Rad.* 4:95-101.
- X-ray Absorption Fine Structure. *Methods in Materials Research* 11.19.
- Yang, B. X., Rivers, M., Schildkamp, W., and Eng, P. J. 1995. GeoCARS microfocusing Kirkpatrick-Baez bender development. *Rev. Sci. Instr.* 66:2278-2280.
- Yun, W. B., Lai, B., Legnini, D., Xiao, Y. H., Chrzas, J., Skulina, K. M., Bionta, R. M., White, V., and Cerrina, F. 1992. Performance comparison of hard X-ray zone plates fabricated by two different methods. *SPIE* 1740:117-129.

## KEY REFERENCES WITH ANNOTATIONS

- Boisseau, P. 1986. Determination of three dimensional trace element distributions by the use of monochromatic X-ray microbeams. M.I.T. Ph.D. Dissertation. *Most complete discussion of x-ray microfluorescence tomography with some early examples.*
- Chevallier, P. and Dhez, P. 1997. Hard X-ray Microbeam: Production and Application. *In Accelerator based atomic physics techniques and applications* (S.M. Shafroth and J. Austin, eds.) pp. 309-348 AIP Press, New York. *Recent overview of x-ray microbeam science and hardware.*
- Ice, G. E. 1997. Microbeam-forming methods for synchrotron radiation. *X-ray Spectrometry* 26:315-326. *Recent overview of x-ray focusing optics for x-ray microprobes with methods for comparing the efficiency of various x-ray focusing optics.*
- Sparks, Jr., C.J. 1980. X-ray Fluorescence Microprobe for Chemical Analysis. *In Synchrotron Radiation Research* (H. Winick and S. Doniach, eds.) pp. 459-512. Plenum, New York 1980. *Quantitative comparison of x-ray microfluorescence analysis to electron and proton microprobes.*
- Stock, S. R., Guvenilir, A., Piotrowski, D. P., and Rek, Z. U. 1995. High resolution synchrotron X-ray diffraction tomography of polycrystalline samples. *Mat. Res. Soc. Symp.* 375:275-280; *Demonstration of the principles of x-ray microdiffraction tomography.*

## ACKNOWLEDGEMENTS

Research sponsored in part by the Laboratory Directed Research and Development Program of the Oak Ridge National Laboratory and the Division of Material Sciences, U.S. Department of Energy under contract DE-AC05-96OR22464 with Lockheed Martin energy Research Corporation. Research carried out in part on beamline 10.3.1 at the ALS and on beamline 2ID at the APS. Both facilities are supported by the U.S. DOE.